ASME Journal of Electronic Packaging
Online journal at:
https://asmedigitalcollection.asme.org/electronicpackaging

Ali Heydari
NVIDIA Corp.,
Santa Clara, CA 95051

Ahmad R. Gharaibeh[1]
Department of Mechanical Engineering,
ES2 Center,
Binghamton University-SUNY,
Binghamton, NY 13902
e-mail: agharai1@binghamton.edu

Mohammad Tradat
NVIDIA Corp.,
Santa Clara, CA 95051

Qusai Soud
Department of Mechanical Engineering,
ES2 Center,
Binghamton University-SUNY,
Binghamton, NY 13902

Yaman Manaserh
NVIDIA Corp.,
Santa Clara, CA 95051

Vahideh Radmard
NVIDIA Corp.,
Santa Clara, CA 95051

Bahareh Eslami
NVIDIA Corp.,
Santa Clara, CA 95051

Jeremy Rodriguez
NVIDIA Corp.,
Santa Clara, CA 95051

Bahgat Sammakia
Department of Mechanical Engineering,
ES2 Center,
Binghamton University-SUNY,
Binghamton, NY 13902

Performance Analysis of Liquid-to-Air Heat Exchanger of High-Power Density Racks

The ability of traditional room-conditioning systems to accommodate expanding information technology loads is limited in contemporary data centers (DCs), where the storage, storing, and processing of data have grown quickly as a result of evolving technological trends and rising demand for online services, which has led to an increase in the amount of waste heat generated by IT equipment. Through the implementation of hybrid air and liquid cooling technologies, targeted, on-demand cooling is made possible by employing a variety of techniques, which include but are not limited to in-row, overhead, and rear door heat exchanger (HX) cooling systems. One of the most common liquid cooling techniques will be examined in this study based on different conditions for high-power density racks (+50 kW). This paper investigates the cooling performance of a liquid-to-air in-row coolant distribution unit (CDU) in test racks containing seven thermal test vehicles (TTVs) under various conditions, focusing on cooling capacity and HX effectiveness under different supply air temperatures (SAT). This test rig has the necessary instruments to monitor and analyze the experiments on both the liquid coolant and the air sides. Moreover, another experiment is conducted to assess the performance of the CDU that runs under different control fan schemes, as well as how the change of the control type will affect the supply fluid temperature and the TTV case temperatures at 10%, 50%, and 100% of the total power. Finally, suggestions for the best control fan scheme to use for these systems and units are provided at the conclusion of the study.
[DOI: 10.1115/1.4065537]

Keywords: data center, high heat density rack, liquid cooling, liquid-to-air heat exchanger, cold plate

1 Introduction

Many essential Internet-scale products and services, such as internet-wide search, email services, and artificial intelligence, have made cloud computing and DCs an essential part of modern life. DC usage has grown dramatically, and there is a larger requirement for downsizing and convergence, which will lead to a rise in the heat load. As a result, their energy usage and negative effects on the environment have grown increasingly substantial. In DC facilities, cooling technologies contribute to 30–50% of the overall energy usage [1,2]. Additionally, it has been shown that about half of DCs' cooling systems are ineffective [3]. An estimated 70×10^9 kWh, or 1.8% of all U.S. power use in 2014, came from data centers in the country [4]. Numerous studies and approaches are used to reduce energy costs. With the American Society of Heating, Refrigeration, and Air-Conditioning Engineers (ASHRAE) allowing a significantly broader acceptable zone, the inlet dry bulb temperature for air entering the IT equipment varies, impacting long-term operation and reliability for air cooling. This temperature range, as specified by ASHRAE TC 9.9, spans from 18 °C to 27 °C, offering guidelines for maintaining optimal conditions within IT environments [5].

[1]Corresponding author.

Contributed by the Electronic and Photonic Packaging Division of ASME for publication in the Journal of Electronic Packaging. Manuscript received January 6, 2024; final manuscript received April 15, 2024; published online June 17, 2024. Assoc. Editor: Ronald Warzoha.

Throughout the past years, air cooling technologies have emerged as the major cooling method. In recent air-cooling studies [6,7] researchers successfully extended the boundaries of air cooling for both 2 U and 4 U form factors, achieving a power dissipation of 500 W per socket. This surpassed conventional air-cooling limits by 150 W, accomplished through the development of an innovative air-cooling solution utilizing thermosyphon heatsinks. However, air-cooled DCs are subject to certain limitations due to the weak thermal characteristics of air, resulting in a suboptimal convective heat transfer coefficient. Moreover, a proper airflow management system is also difficult to implement, and some DCs lack the means to do so [3,8–11]. As a result, data centers started to migrate from traditional air cooling to direct-to-chip cold plate liquid cooling to handle high-density power racks, and it has shown to be a successful, useful, and energy-efficient approach [12–14]. This is due to the fact that liquids with higher specific heat capacities, densities, and incompressibility are able to absorb, store, and transport greater amounts of heat than air [15].

Simon [16] numerically studied the effects of employing rear door air-to-liquid heat exchangers in data centers with low- or high-density racks without an additional cooling method such as computer room air handler (CRAH) or computer room air conditioning units. By developing a computational fluid dynamics model. Gao [17] experimentally investigated the effects of changing supply fluid temperature (SFT), liquid flowrate, and airflow rate on the cooling capability and graphics processing unit case temperatures of a single-phase liquid-cooled IT rack by using liquid-to-liquid CDU. Schmidt [18] used a liquid-to-air HX attached to the side of the server cabinet to minimize the effects of hot air recirculation by absorbing the server heat load of 35 kW without affecting the flow or other components' temperature. Chowdhury [19] was able to identify the benefits and drawbacks of using in-row coolers for different rack power configurations and aisle containment. They also looked into the impact of raising the inlet temperature for IT equipment under various air flow rates and the impact of pairing in-row coolers with external air conditioning units on their cooling capacity. Shahi [20] developed a design of experiment for different heat loads of IT equipment, fluid flowrate, and supply temperature, among other factors that have an impact on the thermal performance and core temperature of liquid-cooled computing systems, and the findings demonstrated a strong connection between the core temperatures and the different input variables. Iyengar [21] conducted an experimental study on the server rack hybrid cooling system, which combines liquid cooling that uses water as the working fluid for high-power components and air cooling for low-power ones at water supply temperatures above ambient. This sort of server lowered overall energy usage by approximately 25% and could tolerate higher coolant inlet temperatures for water and air up to 45 °C and 50 °C, respectively. In another study, Gao [22] offered a detailed approach to examine and explain the HX's transient performance when operating in cooling and heating applications with connected cooling loops or cold plates. They also developed a transient effectiveness technique to assess each component's thermal mass. Bhalerao [23] performed a second-law analysis in computational fluid dynamics to show that the employment of hybrid liquid-air systems can minimize total energy destruction while they enhance energy efficiency. He also found that more heat removal can be achieved by using in-row coolers instead of CRAH units.

This study highlights the adoption of hybrid liquid-to-air in-row HX located inside a row of racks as an alternative to conventional air-cooled solutions for high power-density racks. In this study, the performance of a liquid-to-air in-row CDU was evaluated in terms of the cooling capacity (CC), HX effectiveness, and SFT under different SAT and heat loads. Furthermore, an additional test was conducted to examine the effects of the CDU fan controller modification scheme on various parameters, which include SFT, CDU CC, and case temperatures of the TTVs. The findings of this study have important implications for the design and operation of modern data centers and can help guide the development of more efficient cooling systems for future data center infrastructure.

2 Experimental Setup

The experimental setup used in this study, as seen in Fig. 1, includes three racks: each rack is loaded with six TTVs placed in a 3 U chassis. Each rack is connected to a rectangular cross section rack manifold with air vents on top and two ports at the bottom of each rack manifold attached to the row manifold via coupling stainless steel quick disconnects. A bend port links pipe branches from the rack manifold that goes to the TTV cooling loops, and they are connected via quick disconnects. Two in-row liquid-to-air CDUs with an exact model are connected to a row manifold to supply coolant to the racks. However, in this study, only one CDU was included in the test, and the other one was disconnected from the row manifold. The CDU has two fans and two pumps, one pump is redundant and the rated cooling capacity for the unit is 63 kW and the maximum flowrate is 90 LPM. A propylene glycol mixture with water (PG 25) was the working fluid used in the tests. As an additional method of controlling the liquid flowrate on the secondary side, control valves were installed on the return side of the row manifold of each rack to guarantee that the necessary fluid flowrate was achieved. More details about the experimental setup can be found in Refs. [24] and [25].

Figure 2 shows the schematic of the TTV, cooling loop, and instrumented manifold in the experimental setup. Seven TTVs were used in this study, and each TTV consists of 14 heaters, as seen in Fig. 2(*a*). Eight big heaters (Type X) had a surface area of 50 mm × 50 mm, and each heater can reach a power of 1 kW. Six small heaters (Type Y) had a surface area of 25 mm × 25 mm, and each heater can reach 200 W of total power.

Table 1 summarizes the instrumentation types and specifications that were used in the study.

The cooling loop shown in Fig. 2(*b*) has two types of cold plates: each of the two type X cold plates is in series (for a total of eight cold plates), and the three type Y cold plates are in series (for a total of six cold plates). The coolant is distributed by a common hose (blue hose as seen in Fig. 2(*c*)) for both types of cold plates and returned by a common outlet hose. Fluid distribution through the cooling loop can be used to observe thermal shadowing. As heat is transferred from a cold plate to a coolant, the temperature of the coolant rises, and this decreases the coolant's heat-transfer capacity because the temperature difference between the cold plate's maximum junction temperatures, which represent the temperature at the interface between the cold plate and the heater to the incoming fluid's temperature, is less [26]. The cold fluid enters the even-numbered type X cold plates first and then the preheated fluid flows to the odd ones. While the fluid for the type Y cold plates enters cold plate 1 first, flows to cold plate 2, then enters cold plate 3, and finally leaves via the common hose. Similarly, as in type Y cold plate number 6, it goes to 5 and 4 and then leaves via the common outlet hose.

3 Experimental Procedure

To examine the cooling system's performance in various scenarios when there is no control on the HX fans on the secondary side (no available setpoint for secondary fluid temperature), four test cases were taken into consideration. The outcomes of these tests offer details on how the system operates in a liquid cooling system and serve as a benchmark for comparison under the suggested SAT as per ASHRAE TC 9.9 [27,28] and what are the archived SFT based on these different scenarios and threshold case temperatures of the TTV's heaters. The study was conducted under four different groups of SATs, and at each one, steady-state was reached at 10%, 50%, and 100% of total input power, which represents 6.2, 28, and 60 kW, respectively, with a fixed coolant flowrate of approximately 8 LPM per cooling loop to ensure that the case temperature is below the critical thresholds. The CDU fan PI controller was configured to run at maximum fan integration. More details about the boundary conditions used in the experiments are clarified in Table 2.

4 Results and Discussion

4.1 Coolant Distribution Unit Performance. Four different experiments were conducted to evaluate the performance of the

Fig. 1 The experimental setup used in the study: (*a*) hot aisle containment side, (*b*) cold aisle containment side, and (*c*) schematic diagram of the experimental setup

CDU under different SATs in terms of CDU CC, SFT, CDU fan speed, and CDU pump speed. A steady-state was reached at three different heat loads: 10%, 50%, and 100% at a constant fluid flowrate. Figure 3 shows the results of the four tests at different SATs with cold air measurements taken in the cold aisle containment in front of the CDU by using a grid sensor that consists of 22 °C/ Cambridge AccuSense temperature and velocity sensors. From the results in Figs. 3(*a*), 3(*c*), 3(*e*), and 3(*g*), it can be noted that the SFT depends on the fan speed and heat load, where at low load the fan speed runs at its minimum speed, and as the heat load increases, the fan speed increases to provide sufficient air to cool the liquid in the HX by increasing the air mass flowrate. However, at 50% input power for the four different tests, the fan speed percentage varied, and as the SAT increased, the fan speed percentage also increased for two reasons: the first is to maintain a minimal approach temperature in the HX as the SAT increased and the second reason is to sustain the required mass flowrate for cooling the liquid in the HX. However, the change in fan speed due to change in air density is considered less than 3%. It is also observed that the pumping speed decreases as the heat load increases to maintain a constant coolant flowrate of PG25, where the viscosity of the liquid decreases as its temperature increases, which will cause an increment in the liquid flowrate. In Figs. 3(*b*), 3(*d*), 3(*f*), and 3(*g*), the temperature readings from the temperature sensors for each test indicate the uniformity of the temperature in the cold aisle compared to the setpoint and ensure that there is no recirculation between hot air from hot aisle containment and cold air in cold aisle containment.

4.2 Coolant Distribution Unit Cooling Capacity and Effectiveness. To obtain the cooling capacity of the CDU, the amount of heat removal from each TTV was calculated at the maximum heat

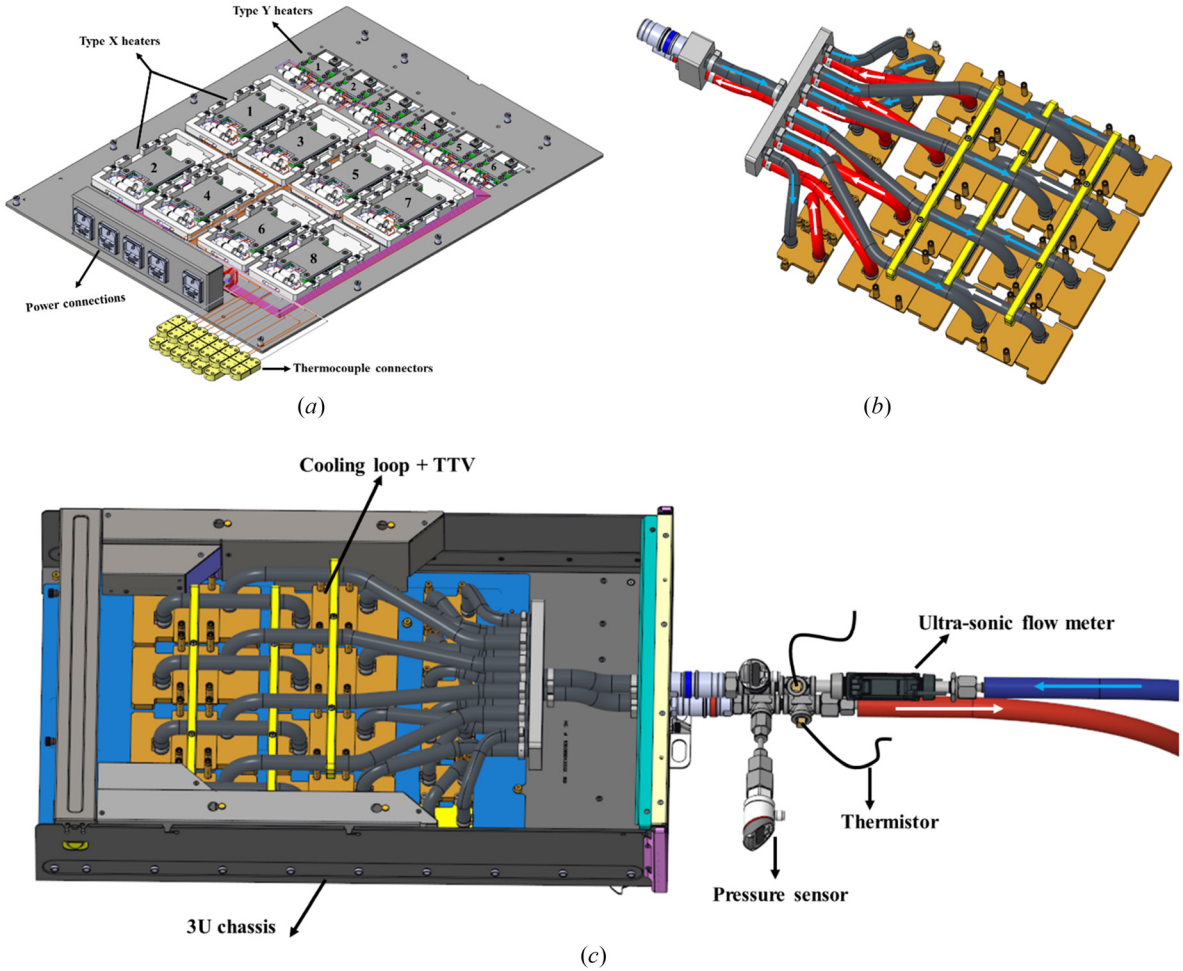

Fig. 2 (*a*) CAD model of the TTV, (*b*) CAD model of the cooling loop, and (*c*) a view of the server shows the TTV heater assembly with cooling loop and instrumented manifold

Table 1 Details of experimental instruments

Description	Specification	Accuracy
Airflow rate	Flow hood multimeter (ADM-850 L)	±3% of reading
Fluid flow rate	FD-X A1 clamp-on microflow sensor	±0.003 ml/min
Data acquisition system	KEYSIGHT DAQ970A	—
Pressure readings	KEYENCE GP-M001T (−14.50–14.50 PSI) KEYENCE GP-M010T (−14.5–145 PSI)	±1% of full scale or less
Power supply	Keysight PS-XHW-200	±0.1%
Air temperature	DegreeC/Cambridge AccuSense ATM2400 airflow temperature monitor	±0.2 °C
Coolant temperature	T-type thermocouples	±0.2 °C

load by using Eq. (1), and then the cooling capacity was found by summation of the amount of heat picked up by the coolant for the seven TTVs by using Eq. (2). The flowrate was measured by using an ultrasonic flowmeter installed at the inlet of each cooling loop attached to the TTV, as well as the coolant inlet and outlet temperatures, by using thermistors at the inlet and outlet sides of the cooling loop manifold, as seen in Fig. 2(*c*).

$$q_{TTV} = \dot{m}_{TTV} C_{p_{PG25}} (T_{Liquid,\,out} - T_{Liquid,\,in}) \quad (1)$$

$$q_{CDU} = \sum_{i=1}^{7} q_{TTV,i} = \dot{m}_{CDU} C_{p_{PG25}} (T_{CDU,\,in} - T_{CDU,\,out}) \quad (2)$$

where q_{TTV} is the amount of heat picked up by the coolant, $\dot{m}_{TTV}$ is the coolant mass flowrate that enters the cooling loop, and $C_{p_{PG25}}$ is

Table 2 Boundary conditions of different tests

Test group	SAT (°C)	Total input power (kW)	Coolant flow rate (LPM)
Group 1	18	6.2	57
		28	
		60	
Group 2	20	6.2	57
		28	
		60	
Group 3	24	6.2	57
		28	
		60	
Group 4	27	6.2	57
		28	
		60	

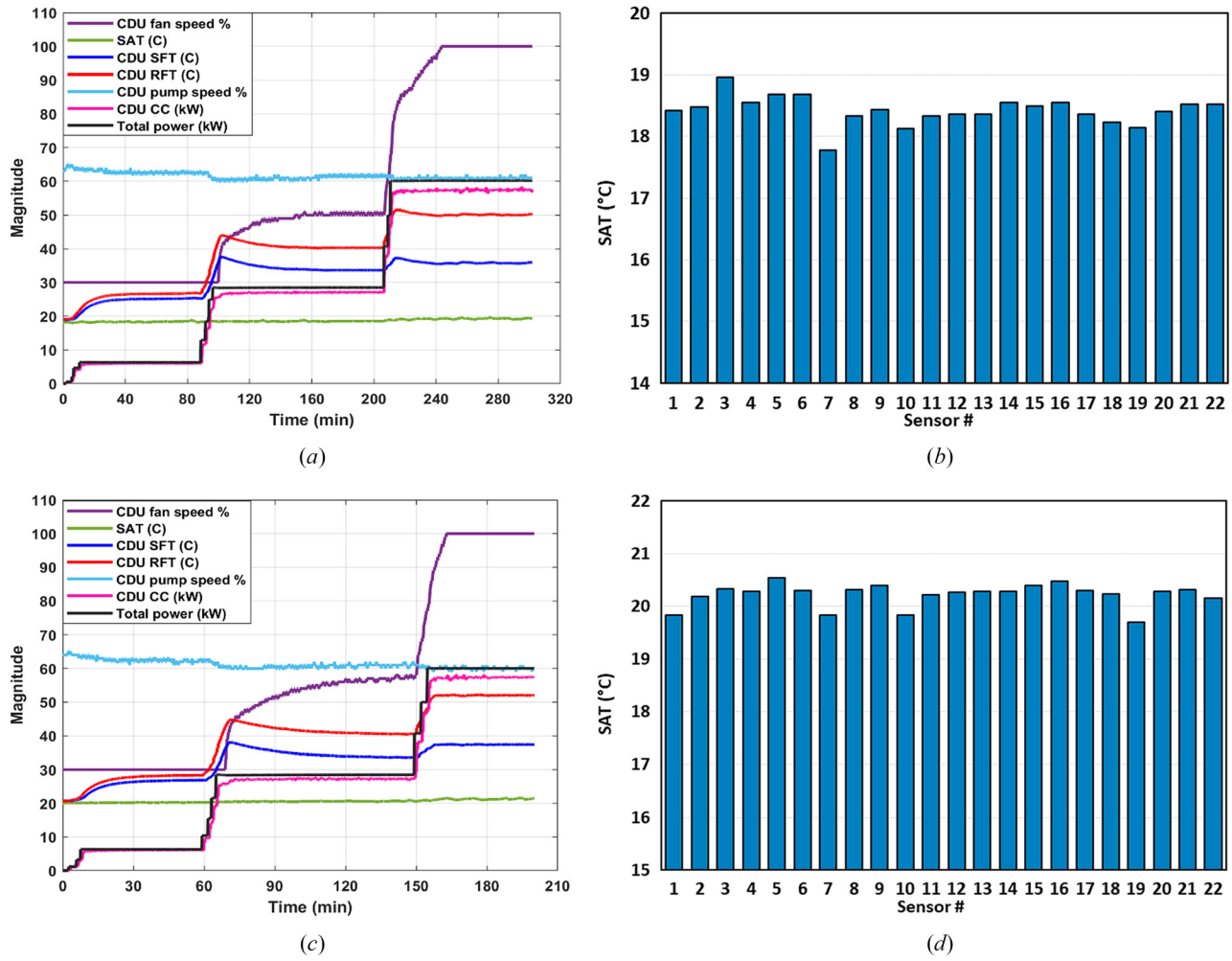

Fig. 3 CDU parameters response with respect to time for different input power levels and SATs. (*a*) CDU response parameters at 18 °C SAT, (*b*) SAT readings from the grid sensors at 18 °C, (*c*) CDU response parameters at 20 °C SAT, (*d*) SAT readings from the grid sensors at 20 °C, (*e*) CDU response parameters at 24 °C SAT, (*f*) SAT readings from the grid sensors at 24 °C, (*g*) CDU response parameters at 27 °C SAT, and (*h*) SAT readings from the grid sensors at 27 °C.

the coolant specific heat. Table 3 shows the measured data of the coolant flowrate and inlet and outlet coolant temperatures in addition to the calculated heat removal from the TTV by the fluid for the first group at 18 °C SAT at a maximum input power of 60 kW.

The HX effectiveness (ε) can be defined as the ratio between the actual heat transfer and the maximum possible heat transfer that might take place if the liquid temperature fell to the SAT. The following correlation can be used to determine the effectiveness of the HX:

$$\varepsilon = \frac{\text{Actual heat transfer}}{\text{Maximum possible heat transfer}} = \frac{\dot{m}_{CDU} C_{p_{PG25}} (T_{CDU,in} - T_{CDU,out})}{(\dot{m}c_p)_{min} (T_{Liquid,out} - T_{air,in})} \quad (3)$$

It should be noted here that the minimum value of $(\dot{m}c_p)$ between the liquid and air should be taken into consideration when finding the maximum possible heat transfer. Figure 4 demonstrates the calculated values of the HX effectiveness at 100% input power in accordance with the achieved values of the SFTs at different SATs. The average value of the HX effectiveness is 0.85, and the SFTs achieved at different SATs are within the range of (35.8–43.3) °C, and the temperature values are less than the upper bound specified by ASHRAE liquid cooling guidelines in the W4 envelope, which is 45 °C within a certain flowrate [27].

4.3 Effects of Fan Control Type. To study the effect of the fan control scheme on the CDU performance in terms of the SFT, cooling capacity, and TTV heater case temperatures, a separate experiment was conducted by the inclusion of six TTVs and a single CDU at the specified boundary conditions of 15 °C SAT, 53 kW input power, and a total fluid flowrate of 44 LPM. The CDU has two types of fan controller modes: proportional-integral mode (PI) and proportional mode (P). For the PI scheme, the fan integration time was changed from 10 to 15 min in steps of 2, and before it reaches the maximum fan integration time, the controller was changed to proportional mode and then returned to PI mode at a fan integration time of 15 min. For a PI controller, the controller output can be found by using the following equation:

$$Z(t) = K_p(SP - PV) + K_I \int (SP - PV)\, dt \quad (4)$$

where K_p is the coefficient for the proportional, SP is the setpoint value, PV is the determined process variable and K_I is the coefficients for the integral.

Figure 5 shows the effect of varying the fan controller on the CDU SFT and cooling capacity. At region A, after the input power increased to the maximum, the CDU fans operated in PI mode with a fan integration time of 10 min, and it can be seen that there is a huge fluctuation in the fan speed, which reflects overshooting in the coolant supply temperature, where the fluctuation's amplitude is

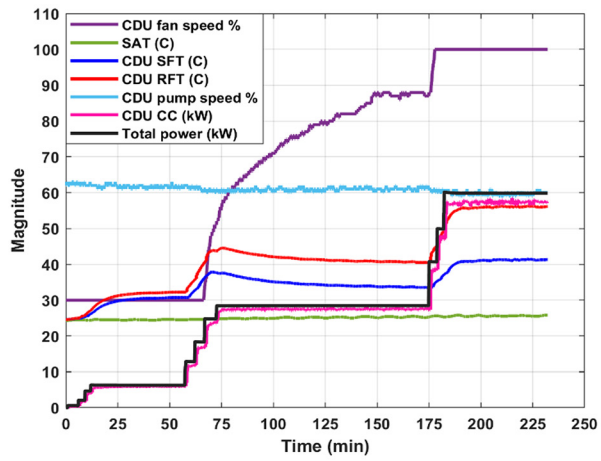

(*e*)

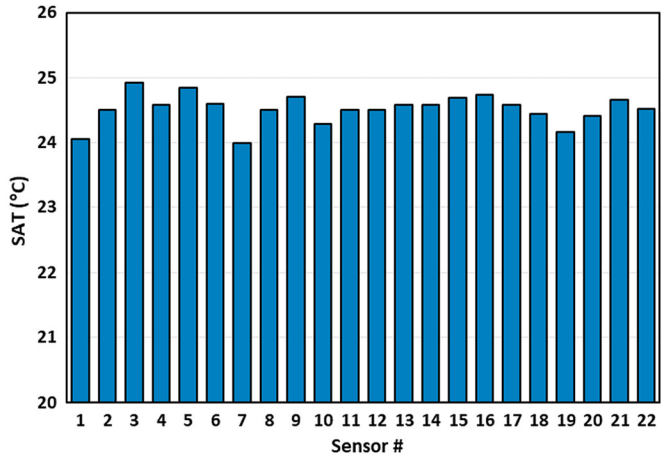

(*f*)

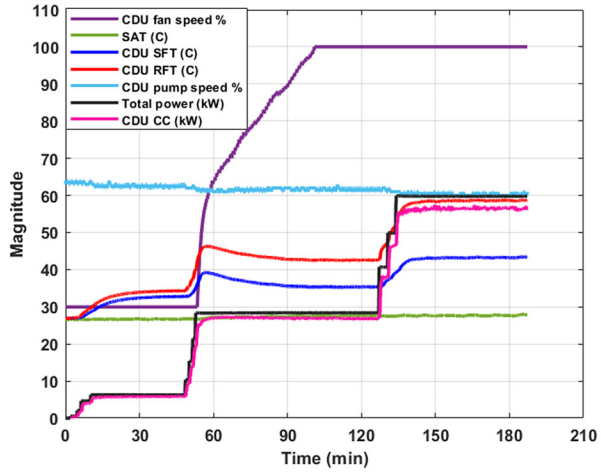

(*g*)

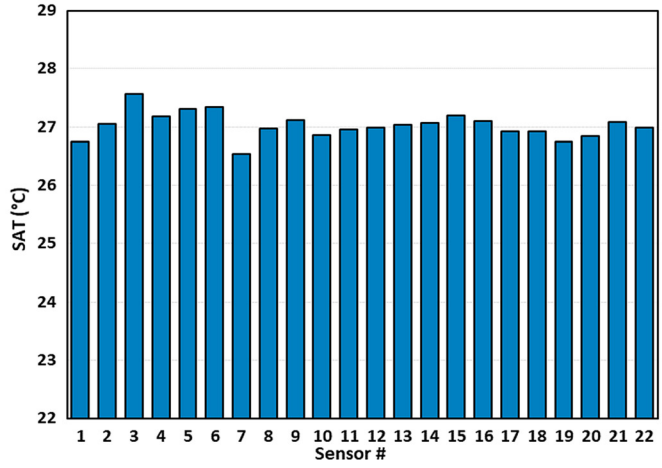

(*h*)

Fig. 3 (Continued)

Table 3 TTVs heat removal data based on the TTV flowrate, inlet and outlet coolant temperatures at 18 °C SAT

TTV #	TTV1	TTV2	TTV3	TTV4	TTV5	TTV6	TTV7
T_{in} (°C)	35.8	35.7	35.8	36	35.7	35.6	36
T_{out} (°C)	50.4	50.7	50.1	51.4	51.3	51.1	51.4
Q (LPM)	7.97	8.25	8.31	8.04	8.1	8.17	8.21
q (kW)	7.8	8.28	7.98	8.3	8.44	8.5	8.46

approximately 2.5 °C. After that, the fan integration time was increased to 12 min and then 14 min, which reduced the oscillation in the fan speed and the amplitude fluctuation of the SFT to around 1.1 °C. In region D, the fan controller was set to proportional type, and the fan speed decreased over time. The SFT increased while the CDU cooling capacity decreased; therefore, we had to change it back to PI to avoid reaching the critical case temperature of the heaters and provide proper cooling to the TTVs. At the final stage in region E, the fan integration time was increased to the maximum, and at this level, the fan oscillation was minimal and a steady SFT was reached with CDU cooling capacity.

Figure 6 demonstrates the response of some of the TTV type X heaters in correspondence to the change in SFT and fan speed percentage due to the change in fan control scheme. Because the SFT depends directly on the fan speed, it will also impact each TTV heater's case temperature. The SFT fluctuated while the fan speed oscillates in regions A, B, C, and D, which caused instability in the case temperature of the heaters with a maximum fluctuation amplitude of 2.8 °C in the case temperature of the heaters. However, in region D, at maximum fan integration time, stable operation for fan speed was achieved, and steady temperatures in the heaters and coolant side were reached.

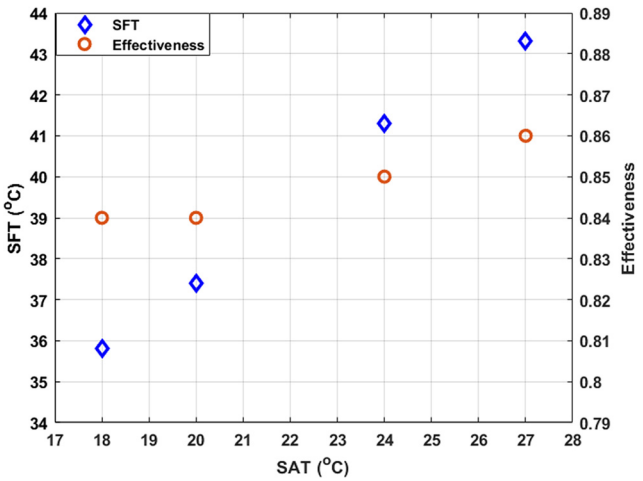

Fig. 4 HX effectiveness values and the archived SFTs at maximum heat load of 60 kW for different SATs

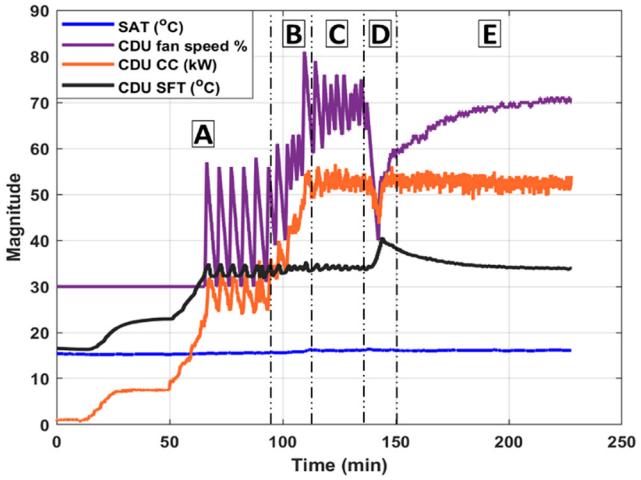

Fig. 5 CDU response parameters in terms of SFT and CC for different PI controllers

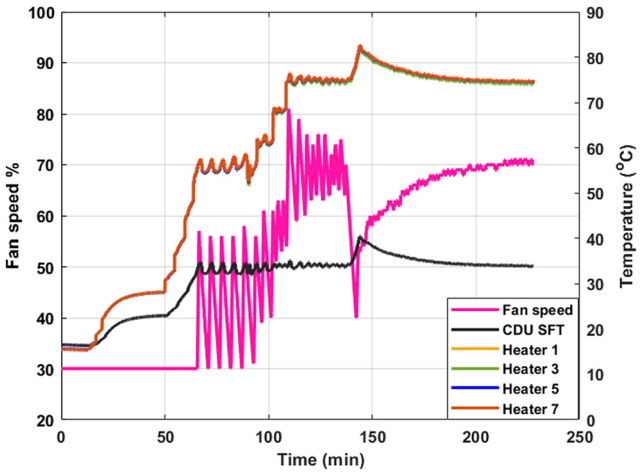

Fig. 6 Case temperatures off odd type X heaters in correspondence to SFT and fan speed at different fan control modes

5 Conclusion

The study investigated the performance of a liquid-to-air implementation in row CDU for high-power density racks under varying heat loads and SATs without any control or setpoint on the secondary loop temperature. The configuration for the liquid cooling system consists of an IT rack filled with TTVs and a liquid-to-air in-row CDU with the necessary instrumentation, and it is used to carry out multiple case studies for experimental characterization. Four different tests were conducted under various SATs (18, 20, 24, and 27 °C); the chosen temperatures were selected based on ASHRAE recommendations for long-term operation and reliability, and steady-states were reached at three different power levels (6.2, 28, and 60 kW). The SFT was found to be dependent on the fan speed and heat load, and at 50% input power, the fan speed percentage varied for each test. It also increased as the SAT increased to guarantee that a sufficient air mass flowrate passed through the HX. The SFTs at various SATs are within the range of 35.8–43.3 °C, and the temperature values are within the highest limit set by ASHRAE liquid cooling recommendations in the W4 envelope, which is 45 °C within a particular flowrate. The average value of HX effectiveness is 0.85. In another experiment, the CDU fan control was changed to study its effects on the SFT, CDU CC, and TTV heater case temperatures, and it was found that at lower fan integration time values, the system is unsteady, and large oscillations in the fan speed result in fluctuation in the SFT and TTV case temperatures. It was concluded that with the PI controller, running the fans at maximum fan integration time is recommended for a stable and steady operation of the system. Overall, this research provides valuable insights into the behavior and performance of liquid-to-air cooling systems in data centers.

Acknowledgment

We would like to acknowledge NVIDIA.

Funding Data

- NVIDIA and NSF (IUCRC Award No. IIIP-2209776 and MRI Award No. CNS1040666; Funder ID: 10.13039/100000001).

Data Availability Statement

The datasets generated and supporting the findings of this article are obtainable from the corresponding author upon reasonable request.

Nomenclature

C_p = specific heat
K_I = integral gain
K_P = proportional gain
$\dot{m}$ = mass flow rate
PV = process variable
q = heat flow rate
Q = volumetric flow rate
SP = setpoint
T = temperature
$Z(t)$ = controller output
ε = heat exchanger effectiveness

Abbreviations

CC = cooling capacity
CDU = coolant distribution unit
CL = cooling loop
CRAH = computer room air handler
DC = data center
HX = heat exchanger
RAT = return air temperature
RFT = return fluid temperature
SAT = supply air temperature
SFT = supply fluid temperature
TTV = thermal testing vehicle

References

[1] Tradat, M. I., Manaserh, Y. M. A., Sammakia, B. G., Hoang, C. H., and Alissa, H. A., 2021, "An Experimental and Numerical Investigation of Novel Solution for Energy Management Enhancement in Data Centers Using Underfloor Plenum Porous Obstructions," Appl. Energy, **289**, p. 116663.

[2] Wang, X., Li, H., Wang, Y., Zhao, J., Zhu, J., Zhong, S., and Li, Y., 2021, "Energy, Exergy, and Economic Analysis of a Data Center Energy System Driven by the CO2 Ground Source Heat Pump: Prosumer Perspective," Energy Convers. Manag., **232**, p. 113877.

[3] Manaserh, Y. M., Tradat, M. I., Gharaibeh, A. R., Sammakia, B. G., and Tipton, R., 2021, "Shifting to Energy Efficient Hybrid Cooled Data Centers Using Novel Embedded Floor Tiles Heat Exchangers," Energy Convers. Manag., **247**, p. 114762.

[4] Shehabi, A., Smith, S., Sartor, D., Brown, R., and Herrlin, M., 2016, "United States Data Center Energy Usage Report," accessed Apr. 14, 2023, https://escholarship.org/content/qt84p772fc/qt84p772fc.pdf

[5] Google Scholar, 2023, "Data Center Power Equipment Thermal Guidelines and Best Practices," accessed Apr. 14, 2023. http://tc0909.ashraetcs.org/documents/ASHRAE_TC0909_Power_White_Paper_22_June_2016_REVISED.pdf

[6] Vincent, M., Ghaffari, O., Nabavi Larimi, Y., Grenier, F., Jasmin, S., Fréchette, L., and Sylvestre, J., 2024, "Experimental Investigation of the Thermal Resistance of Advanced Two-Phase Thermosyphon Heatsinks," Appl. Therm. Eng., **238**, p. 122108.

[7] Ghaffari, O., Vincent, M., Grenier, F., Larimi, Y. N., Jasmin, S., Fréchette, L., and Sylvestre, J., 2023, "Pushing the Limits of Air Cooling With Novel Two-Phase Prototypes for High Power Microprocessors," accessed Mar. 14, 2024,

https://ieeexplore.ieee.org/abstract/document/10177612/?casa_token=rVNo-0SPY-kAAAAA:RFY4d6-6wv49aJB7H_M79iNuCO2NFV9NKrbN66Qb1EpCIVUbjNk1ZAdkSn539PlZ2wElbDZjVJA
[8] Oró, E., Garcia, A., and Salom, J., 2016, "Experimental and Numerical Analysis of the Air Management in a Data Centre in Spain," accessed Apr. 14, 2023. https://www.sciencedirect.com/science/article/pii/S0378778816300366
[9] Dai, J., Ohadi, M. M., Das, D., and Pecht, M. G., 2014, *Optimum Cooling of Data Centers: Application of Risk Assessment and Mitigation Techniques*, Springer, New York, pp. 1–186.
[10] Kadam, S., and Kumar, R., 2014, "Twenty First Century Cooling Solution: Microchannel Heat Sinks," Elsevier, Amsterdam, The Netherlands, accessed Apr. 14, 2023, https://www.sciencedirect.com/science/article/pii/S1290007291400163X?casa_token=1wbE4brXT-4AAAAA:7QgmBX4aNXy_9o0EwZ2foiPsj1ic5NISwBzALA7zIzlyPNgF84HlXvsPRDD2b15DuAg90M3sOxpD
[11] Sauciuc, I., Chrysler, G., Mahajan, R., and Szleper, M., 2003, "Air-Cooling extension - Performance Limits for Processor Cooling Applications," Annual IEEE Semiconductor Thermal Measurement and Management Symposium, San Jose, CA, Mar. 11–13, pp. 74–81.
[12] Gharaibeh, A. R., Manaserh, Y. M., Tradat, M. I., AlShatnawi, F. W., Schiffres, S. N., and Sammakia, B. G., 2022, "Using a Multi-Inlet/Outlet Manifold to Improve Heat Transfer and Flow Distribution of a Pin Fin Heat Sink," ASME J. Electron. Packag., **144**(3), p. 031017.
[13] Tuckerman, D. B., and Pease, R. F. W., 1981, "High-Performance Heat Sinking for VLSI," IEEE Electron Device Lett., **2**(5), pp. 126–129.
[14] Gullbrand, J., Luckeroth, M. J., Sprenger, M. E., and Winkel, C., 2019, "Liquid Cooling of Compute System," ASME J. Electron. Packag., **141**(1), p. 010802.
[15] Radmard, V., Gharaibeh, A. R., Tradat, M. I., Hoang, C. H., Manaserh, Y. Y., Nemati, K., Schiffres, S. N., and Sammakia, B. G., 2023, "Performance Analysis of Corrosion Resistant Electroless Nickel-Plated Impinging Computer Numerical Control Manufactured Liquid Cooling Cold Plate," ASME J. Electron. Packag., **145**(2), p. 021001.
[16] Simon, V. S., Modi, H., Sivaraju, K. B., Bansode, P., Saini, S., Shahi, P., Karajgikar, S., Mulay, V., and Agonafer, D., 2022, "Feasibility Study of Rear Door Heat Exchanger for a High Capacity Data Center," accessed Dec. 4, 2023, https://asmedigitalcollection.asme.org/InterPACK/proceedings-abstract/InterPACK2022/V001T01A018/1153380?casa_token=BqdCvJnmy0wAAAAA:1ZQuZJlB1w73v6So_T93OPwlt_HaHCLa8waYpeWzGTgnuRDLt6RTFbdpyGniaJDUcjs4ofpaXw
[17] Gao, T., Tang, H., and Cui, Y., 2018, "A Test Study of Technology Cooling Loop in a Liquid Cooling System," accessed Apr. 15, 2023, https://ieeexplore.ieee.org/abstract/document/8419519/
[18] Schmidt, R., Iyengar, M., Porter, D., Weber, G., Graybill, D., and Steffes, J., 2010, "Open Side Car Heat Exchanger That Removes Entire Server Heat Load Without Any Added Fan Power," accessed June 28, 2023, https://ieeexplore.ieee.org/abstract/document/5501423/?casa_token=CCCi1PsOjVAAAAAA:at8SWiOd2YdZ_LOjxcIGiSkLi8Dbth8W8tNt87q1qIWLayYWCFtbFx2p6DWx4xBumL1mT_szdfo
[19] Chowdhury, U., Hendrix, W., Craft, T., James, W., Sutaria, A., and Agonafer, D., 2019, "Optimal Design and Modeling of Server Cabinets With in-Row Coolers and Air Conditioning Units in a Modular Data Center," accessed Apr. 15, 2023, https://asmedigitalcollection.asme.org/InterPACK/proceedings-abstract/InterPACK2019/V001T02A009/1071704?casa_token=g0Za9sKN9ucAAAAA:PgUSeqlPRDpyocqKdSYcYDiR2VnFVdUzK8Dipz4dYK8Yl_fe4Zb19YDUqew-eInQXmcHMw6KbA
[20] Shahi, P, Saini, S., Bansode, P., and Agonafer, D., 2021, "A Comparative Study of Energy Savings in a Liquid-Cooled Server by Dynamic Control of Coolant Flow Rate at Server Level," accessed Apr. 15, 2023, https://ieeexplore.ieee.org/abstract/document/9381248/?casa_token=EXMgRhyKF8QAAAAA:otSk-9uabaS9fj3LhCnyDE6vC1kLaW_4zo5WVPnkF7ElRVLh0pYLkuNOBdqIiOoVLktAkWnqdaQ
[21] Iyengar, M., David, M., Parida, P., Kamath, V., Kochuparambil, B., Graybill, D., and Schultz, M., 2012, "Server Liquid Cooling With Chiller-Less Data Center Design to Enable Significant Energy Savings," Annual IEEE Semiconductor Thermal Measurement and Management Symposium, San Jose, CA, Mar. 18–22, pp. 212–223.
[22] Gao, T., David, M., Geer, J., Schmidt, R., and Sammakia, B., 2015, "Experimental and Numerical Dynamic Investigation of an Energy Efficient Liquid Cooled Chiller-Less Data Center Test Facility," Energy Build., **91**, pp. 83–96.
[23] Bhalerao, A., Ortega, A., and Wemhoff, A. P., 2014, "Thermodynamic Analysis of Hybrid Liquid-Air-Based Data Center Cooling Strategies," accessed June 28, 2023, https://asmedigitalcollection.asme.org/IMECE/proceedings-abstract/IMECE2014/V08BT10A080/262039?casa_token=vD0bFOziF7YAAAAA:qGrtOSicgAPnqvYEv9uJv8RSZPP6kl6mppvl4xmXLZO8hWUegE7l8AKfY9a8Q9F_GbbWnbVDnw
[24] Heydari, A., Shahi, P., Radmard, V., Eslami, B., Chowdhury, U., Saini, S., Bansode, P., Miyamura, H., Agonafer, D., and Rodriguez, J., 2022, "Liquid to Air Cooling for High Heat Density Liquid Cooled Data Centers," ASME Paper No. IPACK2022-97386.
[25] Heydari, A., Gharaibeh, A. R., Tradat, M., Manaserh, Y., Soud, Q., Radmard, V., Eslami, B., Rodriguez, J., and Sammakia, B., 2023, "Guidelines and Experimental Hydraulic Performance Evaluation for Single-Phase CDUs Under Steady and Transient Events," InterSociety Conference on Thermal and Thermomechanical Phenomena in Electronic Systems, ITHERM, Orlando, FL, May 30–June 2, pp. 1–5.
[26] Shah, J. M., Dandamudi, R., Bhatt, C., Rachamreddy, P., Bansode, P., and Agonafer, D., 2019, "CFD Analysis of Thermal Shadowing and Optimization of Heatsinks in 3rd Generation Open Compute Server for Single-Phase Immersion Cooling," ASME Paper No. IPACK2019-6600.
[27] Steinbrecher, R., and Schmidt, R., 2011, "Data Center Environments," ASHRAE J., **53**(12), p. e9.
[28] Schmidt, R. R., Belady, C., Classen, A., Davidson, T., Herrlin, M., Novotny, S., and Perry, R., 2004, "Evolution of Data Center Environmental Guidelines," accessed Apr. 24, 2023, http://ancis.us/images/AN-04-9-1.pdf